Tuning of Electrical and Optical Properties of Highly Conducting and Transparent Ta-Doped TiO_2 Polycrystalline Films

Journal:	*The Journal of Physical Chemistry*
Manuscript ID:	jp-2014-126156.R1
Manuscript Type:	Article
Date Submitted by the Author:	05-Mar-2015
Complete List of Authors:	Mazzolini, Piero; Politecnico di Milano, ; Center for Nano Science and Technology-IIT@PoliMI, Gondoni, Paolo; Politecnico di Milano, Russo, Valeria; Politecnico di Milano, Chrastina, Daniel; L-NESS Politecnico di Milano, Physics Casari, Carlo Spartaco; Politecnico di Milano, ; Center for Nano Science and Technology-IIT@PoliMI, Li Bassi, Andrea; Politecnico di Milano, ; Center for Nano Science and Technology-IIT@PoliMI,

Tuning of Electrical and Optical Properties of Highly Conducting and Transparent Ta-Doped TiO_2 Polycrystalline Films

P. Mazzolini, [1,2] *P. Gondoni,* [1] *V. Russo,* [1] *D. Chrastina,* [3] *C.S. Casari,* [1,2] *A. Li Bassi* [1,2]*

[1] Department of Energy - Politecnico di Milano, via Ponzio 34/3, I-20133 Milano, Italy

[2] Center for Nano Science and Technology - IIT@PoliMI, Via Pascoli 70/3, I-20133 Milano, Italy

[3] L-NESS, Dipartimento di Fisica, Politecnico di Milano, Via Anzani 42, I-22100 Como, Italy

* To whom correspondence should be addressed. E-mail: andrea.libassi@polimi.it; tel. +390223996316

Keywords: Transparent Conducting Oxides, Pulsed Laser Deposition, transport properties, anatase, Moss-Burstein effect, electron effective mass.

Abstract

We present a detailed study on polycrystalline transparent conducting Ta-doped TiO_2 films, obtained by room temperature pulsed laser deposition followed by an annealing treatment at 550°C in vacuum. The effect of Ta as a dopant element and of different synthesis conditions are explored in order to assess the relationship between material structure and functional properties, i.e. electrical conductivity and optical transparency. We show that for the doped samples it is possible to achieve low resistivity

(of the order of 5×10^{-4} Ωcm) coupled with transmittance values exceeding 80% in the visible range, showing the potential of polycrystalline Ta:TiO_2 for application as a transparent electrode in novel photovoltaic devices. The presence of trends in the structural (crystalline domain size, anatase cell parameters), electrical (resistivity, charge carrier density and mobility) and optical (transmittance, optical band gap, effective mass) properties as a function of the oxygen background pressures and laser fluence used during the deposition process and of the annealing atmosphere is discussed, and points towards a complex defect chemistry ruling the material behavior. The large mobility values obtained in this work for Ta:TiO_2 polycrystalline films (up to 13 $cm^2V^{-1}s^{-1}$) could represent a definitive advantage with respect to the more studied Nb-doped TiO_2.

1. Introduction

Transparent conductive oxides (TCOs) play a crucial role in the technological evolution of new generation energy conversion devices, such as organic, hybrid or dye sensitized -perovskite solar cells.[1,2] Their development requires new functional properties in order to improve efficiency and durability;[3] in this direction, a high chemical stability and a proper band alignment throughout the material interfaces of the devices is highly desirable for a TCO.[4-7]

One material that could fit these requirements is titanium oxide. Because of its transparency to visible light, high chemical stability in reducing atmosphere and proper band alignment with respect to the active components of the device, TiO_2 is the most employed material as blocking layer and photoanode in dye sensitized solar cells (DSSCs).[8] As a wide band gap oxide, anatase TiO_2 (E_g = 3.2 - 3.4 eV[9,10]) is not an intrinsically good electrical conductor. Interestingly it has been recently discovered that replacing a certain amount of Ti atoms in the titanium oxide tetragonal cell with group V elements, such as Nb or Ta, can strongly reduce the resistivity down to values of the order of 2×10^{-4} Ωcm for epitaxially grown thin films on $SrTiO_3$ substrates.[11,12] Despite the lack of knowledge with respect to the

most studied and widely used TCOs like In_2O_3:Sn, SnO_2:F and ZnO:Al, this new class of d-electron based TCOs seems to have good potentialities.[13,14] In particular, Ta is thought to have definite advantages over Nb in doping TiO_2 for TCO purposes, mainly because of a considerably higher solubility and lower theoretically predicted electron effective mass, which could in principle result in a higher electron mobility.[15] Despite these considerations Ta:TiO_2 (TaTO) is considerably less studied than Nb:TiO_2 (NTO).[11,16-27] In particular only a few works have been devoted to the control of electrical/optical properties of TaTO polycrystalline thin films on cheap substrates (e.g. soda-lime glass),[28-30] which is a crucial requirement in view of a possible application in real devices, such as DSSCs. To the best of our knowledge, the lowest resistivity values at room temperature obtained so far for polycrystalline NTO and TaTO thin films are respectively 4.6×10^{-4} Ωcm and 8.7×10^{-4} Ωcm.[17,30] In order to obtain highly conductive polycrystalline TiO_2-based TCOs, it is necessary to use a two-step approach, which involves the deposition of amorphous films (*e.g.* by pulsed laser deposition or sputtering) followed by a post-deposition treatment in reducing atmosphere (vacuum or H_2). A reducing deposition atmosphere is a basic requirement also for the synthesis of highly conductive epitaxial films. However, the defect chemistry and its role in determining the functional properties are still open issues for this new class of TCOs.[27-29,31-34]

The typical limitations in polycrystalline TiO_2-based TCOs are connected to lower obtainable mobility values with respect to the epitaxially grown films. In fact, for an optimal extrinsic doping level (5% and 6% for Ta and Nb respectively[12,35]), it is usually possible to obtain large charge carrier densities (usually in the range of 5 to 15×10^{20} cm^{-3}) for both epitaxial and polycrystalline thin films, while the mobility value is more than halved due to the presence of different domain orientations (from values in the range of 20 $cm^2V^{-1}s^{-1}$ for epitaxially grown films, down to values in the range of 5 $cm^2V^{-1}s^{-1}$ for randomly oriented polycrystalline films).[11,12,17-19,22,25,28,30,36-40]

One of the most suitable and versatile synthesis techniques in order to finely control the structure/property relation in doped oxide thin films is pulsed laser deposition (PLD).[41] In this work we systematically explore the optimization of both the electronic transport and optical transparency of polycrystalline TaTO thin films deposited via PLD, in order to unveil the real potentialities of TaTO, with particular interest on the possible advantages with respect to the better explored NTO.[15]

TaTO films on soda-lime glass substrates have been obtained at room temperature by tuning the oxygen background pressure and the laser fluence during the ablation process, and were then annealed in different atmospheres (air and vacuum). We were able to obtain extremely low resistivity values of the order of 5×10^{-4} Ωcm and transmittance in the visible region above 80%. Hall effect and absorbance measurements were used to evaluate the electron conduction band effective mass. The obtained electrical and optical properties are discussed in light of the material structural features, which can be adjusted by tuning the different synthesis parameters (oxygen background pressure during the deposition process, laser fluence, annealing atmosphere). The high electron mobility data are analyzed in comparison to the most investigated Nb-doped TiO_2.

2. Experimental Section

TaTO (Ta = 5% at.) and TiO_2 thin films were grown by PLD on soda-lime glass and Si(100) substrates kept at room temperature, by ablating respectively Ta_2O_5:TiO_2 (molar ratio 0.025:0.975) and TiO_2 solid targets with a ns-pulsed laser (Nd:YAG 4th harmonic, λ = 266 nm, repetition rate f_p = 10 Hz, pulse duration ~ 6 ns). The energy density was varied from 0.9 to 1.5 J/cm^2 by changing the focused area on the surface of the solid target (laser pulse energy measured before the focusing lens was kept at 75 mJ), while the target-to-substrate distance was fixed at 50 mm. Where not otherwise specified we will refer in the following to a fluence of 0.9 J/cm^2. All the depositions were made in oxygen background

pressure; TaTO films were deposited in the range 0.9 - 2.25 Pa, while TiO_2 films were deposited at 1 and 1.25 Pa.

All the as-deposited TiO_2-based thin films were amorphous. In order to obtain single phase polycrystalline anatase, we exploited a post deposition annealing treatment in vacuum atmosphere ($p < 4\times10^{-5}$ Pa) in a home-made furnace at 550°C (10°C/min ramp, 1 hour dwell) and in air at 550°C in a Lenton muffle furnace (8°C/min ramp, 1 hour dwell).

Film thickness was evaluated by means of scanning electron microscopy (Zeiss SUPRA 40 field-emission SEM) on samples grown on silicon.

The crystalline structure has been determined by micro-Raman measurements (Renishaw In Via spectrometer with Ar^+ laser, λ = 514.5 nm – power on sample 1 mW) and x-ray diffraction (PANalytical X'Pert PRO MRD high-resolution X-ray diffractometer, using CuKα1 radiation (λ = 0.15406 nm) selected by a two-bounce Ge monochromator). XRD measurements were performed in both θ-2θ and grazing incident angle configuration (fixed incident angle ω = 5°). The lattice parameters and the mean crystalline domain size were determined by evaluating peak positions and full width at half maximum in grazing incidence angle configuration, since grazing scans gave more intensity for the analyzed peaks. The thin film surfaces were investigated by means of optical microscopy (Leitz orthoplan-pol).

The electrical characterization was performed in the 4-point probe configuration with a Keithley K2400 Source/Measure Unit as a current generator (from 100 nA to 10 mA), an Agilent 34970A voltage meter and a 0.57 T Ecopia permanent magnet.

Optical transmittance and reflectance spectra (in the range 250 - 2000 nm) were evaluated with a UV–vis–NIR PerkinElmer Lambda 1050 spectrophotometer with a 150 mm diameter integrating sphere. All

the acquired spectra were normalized with respect to the glass substrate contribution by setting to 1 the intensity at the glass/film interface.

3. Results

3.1. Structural properties

TaTO and TiO_2 SEM micrographs show a similar 'compact' morphology for all the samples (a TaTO micrograph is shown in Figure 1). All the TaTO thin films grown at different O_2 pressure are characterized by the same thickness of 150 ± 5 nm, while the TiO_2 ones are 250 ± 5 nm and 150 ± 5 nm thick (for 0.9 and 1.15 J/cm^2 laser fluence respectively).

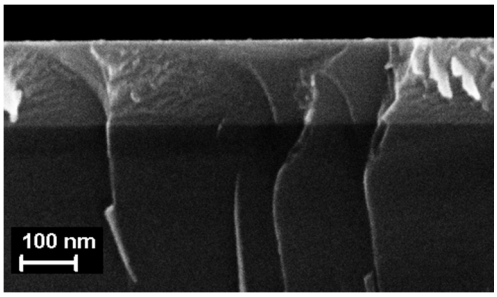

Figure 1. SEM micrograph of 150 nm thick vacuum annealed TaTO (1.25 Pa oxygen background deposition pressure) on Si substrate.

Raman spectroscopy was employed to analyze the structure of the films. All the acquired spectra for the room temperature deposited samples are similar, showing broad bands typical of amorphous / highly disordered titanium oxide (black line in Figure 2). On the other hand, five distinct peaks related to the expected anatase active modes are present in the Raman spectra of all annealed films, regardless of the annealing atmosphere. In Figure 2 (red line) it is possible to identify the three E_g modes at 144 cm^{-1}, 197 cm^{-1} and 639 cm^{-1}, the B_{1g} mode at 399 cm^{-1} and the peak at 519 cm^{-1}, due to superposition of the remaining A_{1g} and B_{1g} modes.[42,43] We may conclude that both the annealing processes in air and vacuum atmosphere (T = 550°C) are efficient to crystallize the TiO_2-based films in the anatase phase.

Moreover for all the acquired spectra there is no evidence of rutile Raman modes, excluding the formation of this phase under the used annealing conditions.

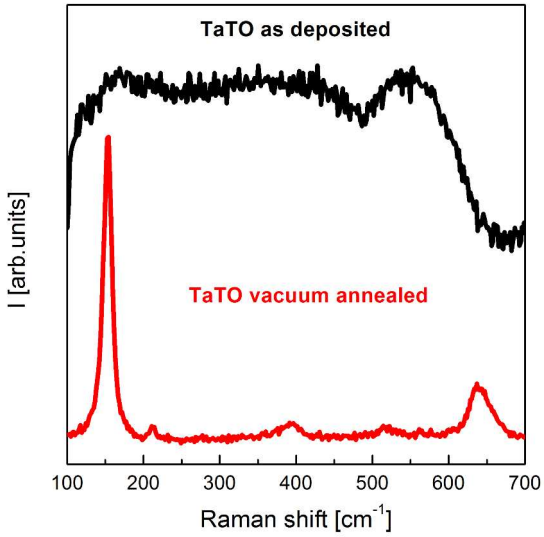

Figure 2. Raman spectra of as-deposited (black line) and vacuum annealed (red line) TaTO thin films deposited at 1.25 Pa oxygen background pressure.

The presence of anatase crystalline phase only for all the annealed films is confirmed by XRD measurements. As an example, selected XRD diffraction patterns for vacuum annealed samples deposited at two different oxygen background pressures (1.25 and 2 Pa) are shown in Figure 3 *(a)*, together with the XRD pattern of an undoped TiO_2 film. No rutile peaks are observed, as well as tantalum oxide (Ta_2O_5) or metallic tantalum segregations. The crystalline quality of the vacuum annealed TaTO films seems to be dependent on the oxygen background pressure during the deposition process. In fact we are able to identify a narrow window of deposition pressures between 1.25 and 1.75 Pa in which both the most intense diffraction peaks of the anatase phase ((101) and (200)) are observed in θ-2θ configuration (see e.g. red line in Figure 3 *(a)*), while at lower (1 Pa) and higher (2 – 2.5 Pa) deposition pressures a significant decrease of the (101) anatase reflection intensity is detected (see e.g. purple line in Figure 3 *(a)*).

Moreover, for the most crystalline samples deposited in the above mentioned pressure window (1.25 – 1.75 Pa), the introduction of Ta atoms in the crystal lattice seems to increase the intensity of the (101) peak and simultaneously decrease the (200) peak with respect to undoped TiO_2, in the θ-2θ configuration (see e.g. red line and blue line in Figure 3 *(a)*). For undoped titanium oxide it is known that, since the <101> surface has the lowest surface energy,[44] anatase thin films grown on amorphous substrates can result in either randomly oriented or <101> preferred-oriented polycrystalline forms.[45] In our case, the variation in the intensity ratio of anatase x-ray reflections could be related to an effect of doping or defect-induced lattice distortion or disordering (see Section 4 - Discussion).

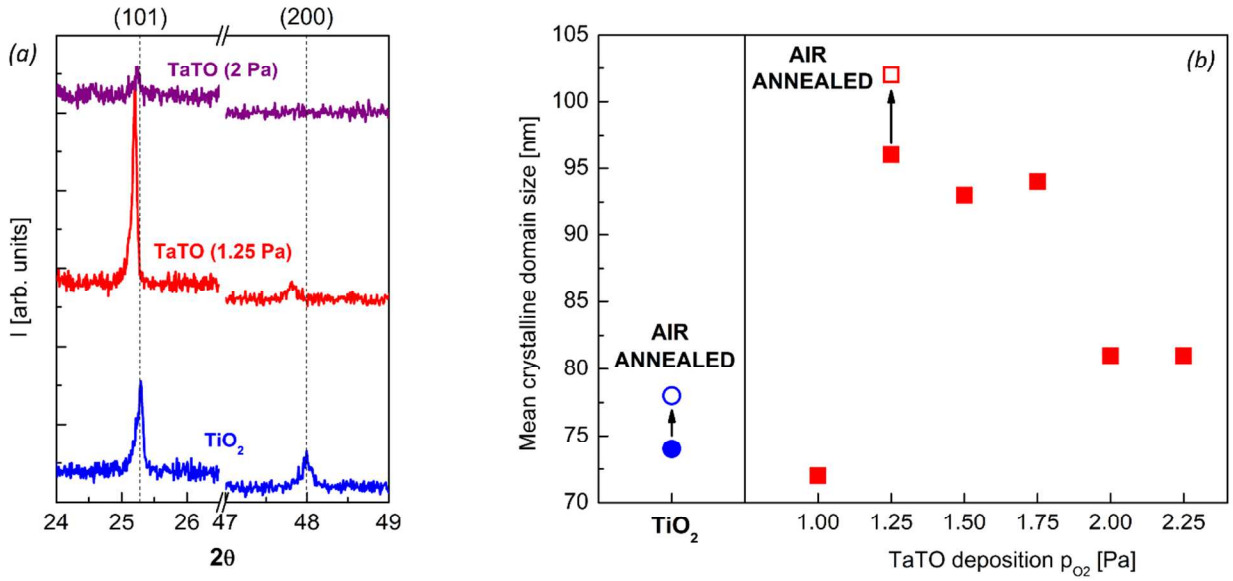

Figure 3. *(a)* XRD diffraction patterns of vaccum annealed TiO_2 (blue line) and TaTO thin films deposited at different oxygen background pressures (1.25 – 2 Pa respectively red and purple line). *(b)* Mean crystalline domain size evaluated from XRD of TiO_2 (blue spot on the left side) and TaTO samples deposited at different oxygen partial pressure (red squares), vacuum (filled) and air (empty) annealed at 550°C.

Furthermore, comparing XRD peak positions for vacuum annealed undoped and Ta doped TiO_2 samples, it is possible to identify the presence of a shift to smaller angles for the doped samples (as visible in Figure 3 *(a)*). This could be partially ascribable to a lattice expansion due to Ta incorporation

in substitutional Ti sites, since the ionic size of Ta^{+5} (0.064 nm) is slightly larger than that of Ti^{+4} (0.061 nm).[12,46] Nevertheless the shift is also dependent on the oxygen background pressure used in the deposition process; in particular the shift reduces as the oxygen deposition pressure is increased. This will be further discussed in Section 4 (Discussion).

In grazing incident configuration (fixed incidence angle $\omega = 5°$), both (101) and (200) diffraction peaks are detected for all the range of TaTO deposition pressures, with a stronger intensity with respect to θ-2θ measurements (not shown), and were employed to evaluate the mean crystalline domain size according to Scherrer equation (Figure 3 *(b)*). The above mentioned narrow window of deposition pressures (between 1.25 and 1.75 Pa) is confirmed to be the one with the higher diffraction peaks intensity also in grazing incident configuration.

Domain size values for the vacuum annealed samples are reported in Figure 3 *(b)* (filled symbols), showing larger values for deposition pressures in the range 1.25 – 1.75 Pa, thus confirming the discussed 'good crystallinity' window. We also observe that the domain size for Ta-doped films is larger or comparable with that found for undoped TiO_2. The same analysis shows that a post crystallization process in the presence of oxygen (annealing in air) increases the mean domain size with respect to the vacuum annealing process (domain size respectively 78 and 102 nm for TiO_2 and TaTO deposited at an oxygen background pressure of 1.25 Pa, empty symbols in Figure 3 *(b)*).

While the Scherrer equation provides an evaluation of the mean crystalline domain size in the almost-vertical direction (which is basically limited by the film thickness), an optical microscopy analysis of the thin film surface of vacuum annealed TaTO samples deposited at different oxygen pressures allows the evaluation of the grain size in the horizontal plane (Figure 4). Circular macro-cracks are only observed on the surface of TaTO deposited at 1 Pa (Figure 4 *(a)*), while for higher deposition pressures the presence of macro-grains is clearly visible, as already observed by Pore *et al.*[47] for the post

crystallization from amorphous phase of Nb- and Ta-doped TiO_2 films; in particular the macro-grain dimension is following the trend obtained from the XRD analysis (Figure 3 *(b)*): in the narrow window of deposition pressures for which the XRD crystalline domain size is larger, the grain size is of the order of 25-30 μm (1.25-1.5-1.75 Pa, Figure 4 *(b)*), while for higher deposition pressures (2-2.25 Pa) the typical grain size decreases down to 10-15 μm (Figure 4 *(c)*). This evidences are providing an indication of the good crystallinity of the films.

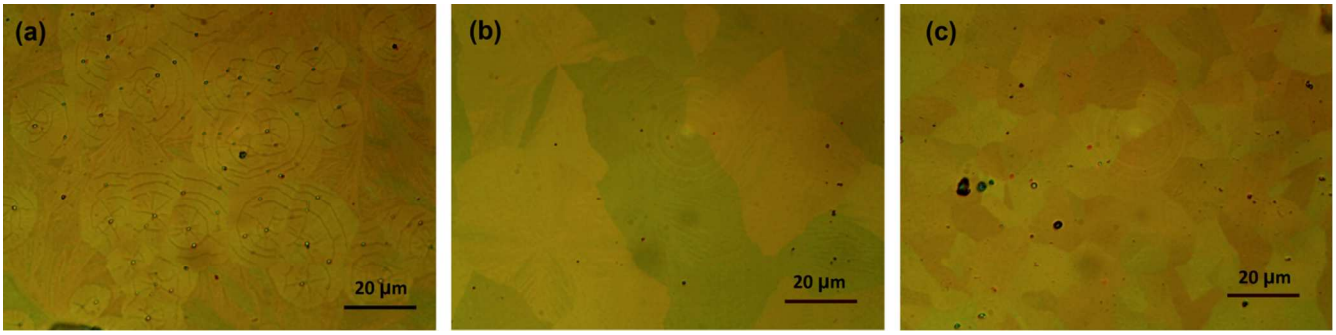

Figure 4. Surface images captured using polarized light through optical microscope of vacuum annealed TaTO films deposited at 1 Pa *(a)*, 1.5 Pa *(b)* and 2.25 Pa *(c)*.

3.2. Electrical properties

The as-deposited films have a typical resistivity value in the order of 10 Ωcm without showing any particular tendency with respect to the presence of doping or different oxygen deposition pressure. For such measurements it was not possible to discern the contributions of charge carrier concentration and charge mobility because of the highly scattered values obtained in Hall measurements.

The post-deposition crystallization process in vacuum drastically decreases the resistivity values for all the samples, as reported in Figure 5 where we show resistivity for undoped TiO_2 and TaTO (1.25 Pa O_2), as-grown and after annealing. Undoped TiO_2 exhibits a drop of nearly 3 orders of magnitude, reaching a resistivity value comparable with the best results obtained for PLD epitaxially grown films.[48] The TaTO film with the best electrical properties (grown at 1.25 Pa O_2) showed a resistivity

value of $\rho = 5.73\times10^{-4}$ Ωcm (see Figure 5) and sheet resistance $R_S = 38$ Ω/□; to the best of our knowledge, the resistivity value for the TaTO thin film is the lowest reported in literature for a tantalum-doped TiO_2 polycrystalline film and in line with the best results obtained with the most investigated NTO.[17,28,30,49]

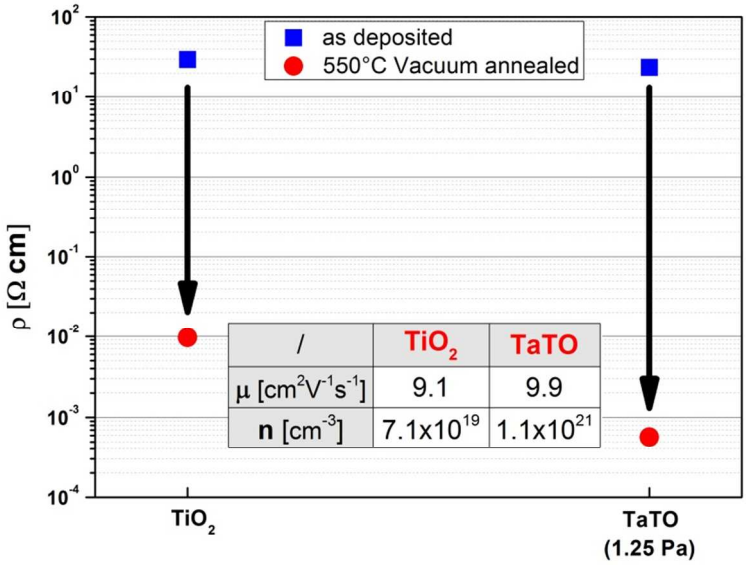

Figure 5. Effect on resistivity of the crystallization process exploited in vacuum atmosphere for TiO_2 and TaTO (deposited in an oxygen background pressure of 1.25 Pa). The resistivity values for the as deposited films are represented with blue squares, while the crystallized ones with red circles. In the inset table are reported mobility and electron density of the vacuum annealed samples.

The data reported in the inset of Figure 5 show that the difference between the electrical properties of vacuum annealed doped and undoped thin films mainly resides in the charge carrier density, which for TaTO is more than one order of magnitude higher, while the measured mobility is comparable. Still it is interesting to underline the possibility to obtain such a high concentration of free electrons in undoped TiO_2: due to the absence of an extrinsic dopant, this evidence should be strictly related to the presence in the anatase cell of a large amount of oxygen vacancies, which are known to effectively act as electron donors.[50]

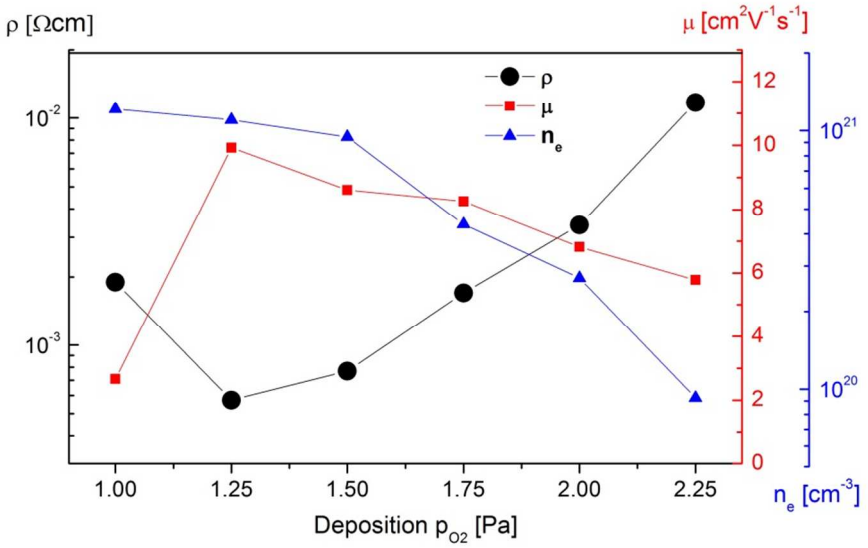

Figure 6. Electrical properties of polycrystalline TaTO thin films (150 nm) deposited in different oxygen partial pressures and annealed in vacuum atmosphere (550°C). The black spots represent the resistivity, the blue triangles represent the electron density, and the red squares represent the electron mobility evaluated via Hall measurements.

Furthermore, for TaTO vacuum annealed samples, we found a strong dependence between the electrical properties and the oxygen background pressure used during the deposition process. As visible in Figure 6, resistivity values decrease by more than one order of magnitude while oxygen pressure decreases from 2.25 Pa to 1.25 Pa and increase again with a further pressure reduction to 1 Pa. In the same figure the variation of conduction electron density and mobility versus oxygen deposition pressure is also reported. The decrease in electrical properties of the film deposited at 1 Pa is connected to the drop of electron mobility (respectively 2.7 and 9.9 $cm^2V^{-1}s^{-1}$ for 1 and 1.25 Pa), in spite of the highest conduction electron density (respectively 1.21×10^{21} and 1.1×10^{21} cm^{-3} for 1 and 1.25 Pa).

In order to explore the optimization of the deposition process, the effect of a different laser fluence for TaTO and TiO_2 thin films was also explored. As the amount of ablated material is related to the energy density on target surface, it was necessary also to tune the oxygen background pressure during the ablation process in order to optimize electrical properties. Finally it was found that for 1.15 and 1.5

J/cm^2 laser fluences the best electrical properties for TaTO vacuum annealed films could be obtained for 1 Pa oxygen pressure (with respect to the 1.25 Pa optimum condition found for the 0.9 J/cm^2 fluence). The use of a higher laser fluence slightly increases the resistivity of the films (from 5.73×10^{-4} to 6.47×10^{-4} Ωcm, see Figure 7) due to a small decrease in the free electron density. On the other hand by tuning the fluence it is possible to strongly enhance the electron mobility: for a TaTO 150 nm thick deposited at a laser fluence of 1.15 J/cm^2 (1 Pa O_2) it was possible to obtain $\mu = 12.5$ cm^{2}V^{-1}s^{-1} ($\rho = 5.90\times10^{-4}$ Ωcm, $n = 8.49\times10^{20}$ cm^{-3}, $R_S = 39.3$ Ω/□). For comparison we studied also a vacuum annealed TiO_2 150 nm thick film deposited at the same laser fluence, which showed as well a noticeable increase in the electron mobility ($\rho = 6.46\times10^{-3}$ Ωcm, $n = 6.16\times10^{19}$ cm^{-3}, $\mu = 15.7$ cm^{2}V^{-1}s^{-1}).

Finally we verified that the electrical properties are almost independent with respect to the TaTO film thickness: this provides the possibility of tuning the sheet resistance. In fact by almost doubling the thickness (295 nm) and maintaining the same laser fluence (1.15 J/cm^2), we were able to obtain almost the same resistivity ($\rho = 5.57\times10^{-4}$ Ωcm, $\mu = 13.0$ cm^{2}V^{-1}s^{-1}, $n = 8.61\times10^{20}$ cm^{-3}) and consequently the sheet resistance dropped down to 18.9 Ω/□. It is interesting to note that the mobility values reported in this work are significantly larger than those reported in literature for polycrystalline films of doped TiO_2.[17,19,37,38,51]

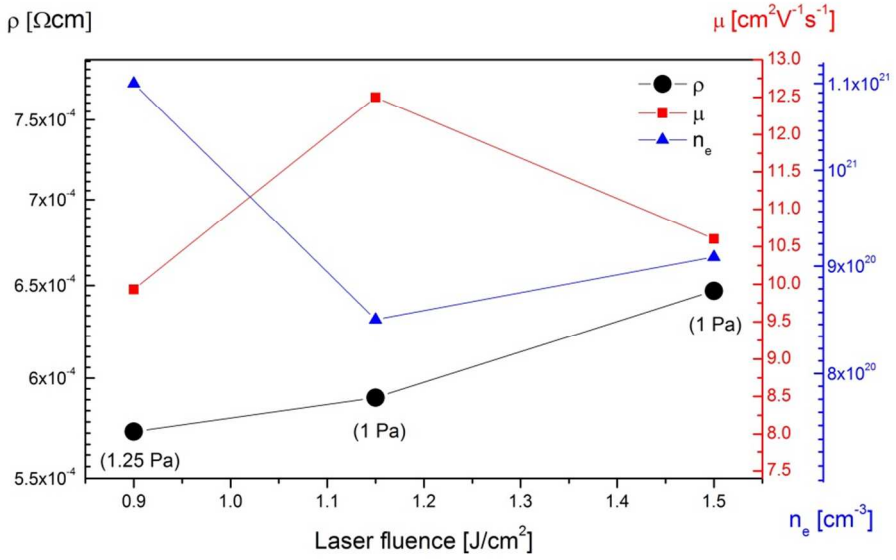

Figure 7. Electrical properties of TaTO films (150 nm) deposited at different laser fluence and vacuum annealed at 550°C. In the brackets are reported the oxygen deposition pressures. The black spots represent the resistivity, the blue triangles represent the electron density and the red squares represent the electron mobility evaluated via Hall measurements.

As clear from the behavior of vacuum annealed TaTO films deposited at different background pressures, oxygen clearly plays a key role in determining the electrical properties; this is confirmed by performing the crystallization process in air, which is known to be highly detrimental for both TiO_2 and TaTO thin films.[35] In fact, with our experimental setup, it was not possible to measure the resistivity (as well as the resistance in 2-point configuration measurements), suggesting a resistance of all the air-annealed films higher than 10 GΩ.

3.3. Optical properties

As well as structural and electrical properties, the optical properties of TaTO thin films also appear to be related to the oxygen background pressure during the deposition process. In Figure 8 total transmittance spectra for vacuum annealed TaTO films are reported, highlighting a tendency towards higher transmittance for higher oxygen background pressures during the deposition process. This is particularly evident in the near-IR region, where the absorption is due to plasma oscillations of the

"free" conduction band electrons (according to the Drude model), and lower transmittance at lower pressures should be related to higher free electron density values (see Figure 6). Moving to lower wavelengths it is possible to observe the presence of interference fringes in the visible range, whose position and spacing is related to the film thickness and refractive index, and then a sharp drop in the UV region because of the crossing of the optical band gap.

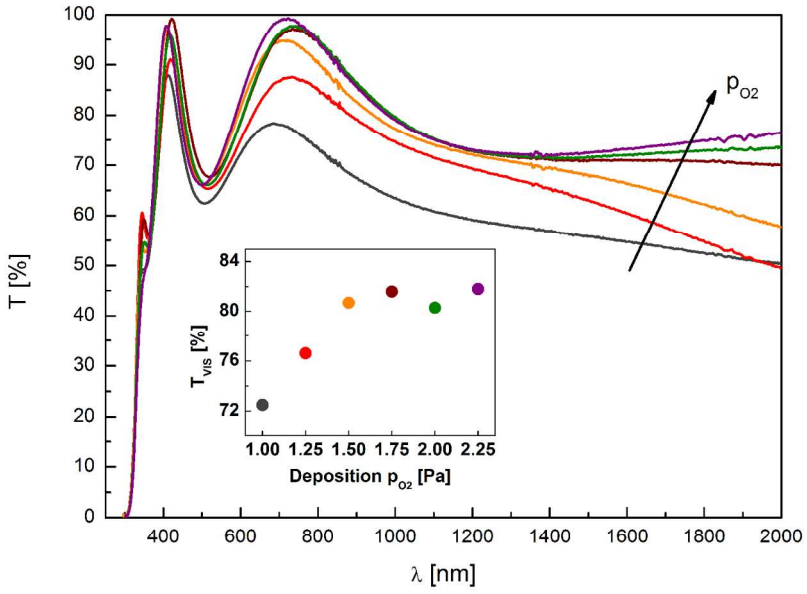

Figure 8. Total transmittance spectra of 150 nm thick TaTO films deposited with different oxygen partial pressures and annealed in vacuum atmosphere (550°C).In the inset graph the mean transmittance values evaluated in the visible region (λ = 400 – 700 nm) are reported as a function of different oxygen deposition pressures.

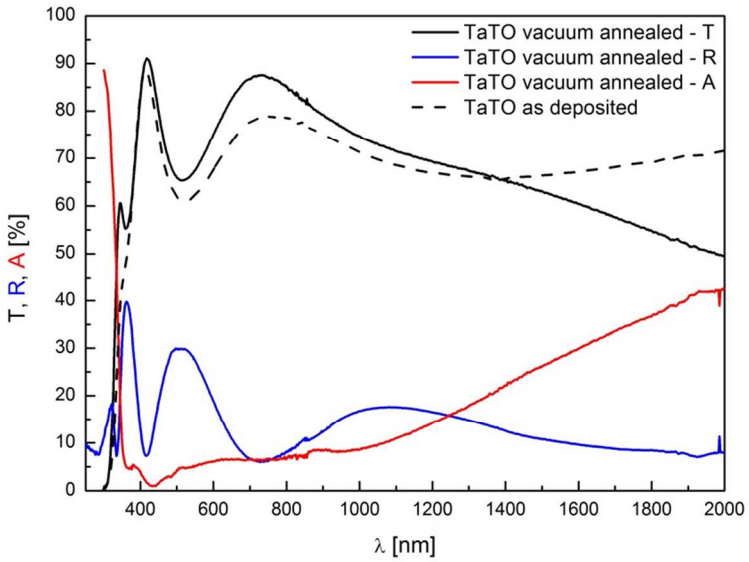

Figure 9. Total transmittance (black line), reflectance (blue line) and absorbance (red line) spectra of 150 nm thick TaTO film deposited at an oxygen partial pressure of 1.25 Pa annealed in vacuum atmosphere (550°C). The black dotted line refers to the total transmittance of the same sample before the crystallization process.

From the transmittance spectra the mean transmittance in the visible range (T_{VIS} for $\lambda = 400 – 700$ nm) can be calculated, finding in general higher values for higher oxygen background pressure during the deposition process (inset of Figure 8). For the TaTO vacuum annealed film deposited at 1.25 Pa, which shows the best electrical properties ($\rho = 5.73\times10^{-4}$ Ωcm), T_{VIS} is 76.6%. For this 'best' film we report in Figure 9 the transmittance, reflectance, and absorbance spectra, together with the transmittance spectrum of the amorphous as deposited film. The comparison reveals that the obtained mean transmittance value in the visible region is strongly dominated by reflectance (R_{VIS} = 18.7%), while absorption is as low as 5%. We also note that the as-deposited amorphous film (dotted line in Figure 9) does not show the absorption in the near-IR due to plasma oscillations of the "free" conduction band electrons.

We also studied the effect of the annealing process in air on the optical properties, finding that for TaTO films deposited at 1 and 1.25 Pa, T_{VIS} is enhanced up to 79.9% and 80.0% respectively, while for

oxygen background pressures higher than 1.25 Pa, T_{VIS} values remained almost unchanged regardless of the annealing atmospheres. This fact could be related to the presence of a higher concentration of oxygen vacancy defects for the vacuum annealed TaTO deposited at lower oxygen pressures (1 – 1.25 Pa), as it is known that this occurrence usually leads to a decrease in the total transmittance values.[52,53]

Finally we investigated the effect of the laser fluence on the optical properties of 150 nm thick TaTO films. In particular, for the sample deposited at a laser fluence of 1.15 J/cm^2 (see Figure 10 *(a)*), we were able to obtain an increase of the total transmittance in the visible range of nearly 5% (T_{VIS} = 76.6% and 81.1% respectively for 0.9 J/cm^2 and 1.15 J/cm^2), even though they maintain almost the same electrical resistivity ($\rho = 5.73\times10^{-4}$ Ωcm and 5.90×10^{-4} Ωcm respectively for 0.9 J/cm^2 and 1.15 J/cm^2).

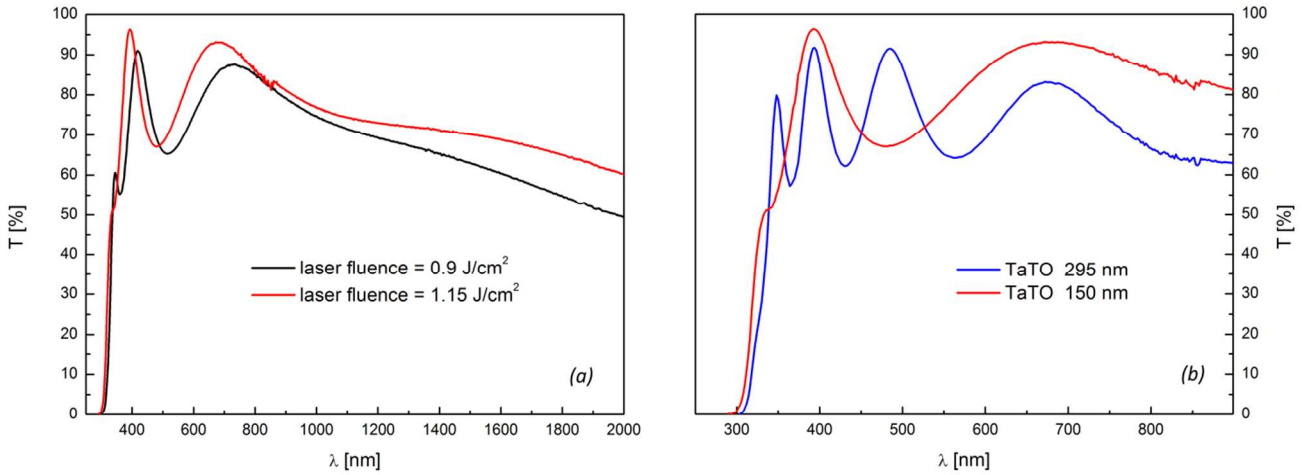

Figure 10. *(a)* Total transmittance spectra of 150 nm thick TaTO films deposited at a different laser fluence (0.9 and 1.15 J/cm^2) annealed in vacuum atmosphere (550°C). *(b)* Total transmittance spectra of 150 and 295 nm thick TaTO films deposited at a laser fluence of 1.15 J/cm^2 annealed in vacuum atmosphere (550°C).

As for the thickness effect on the total transmittance, a nearly doubled thickness of 295 nm with respect to the 150 nm thick TaTO already shown in Figure 10 *(a)* (laser fluence 1.15 J/cm^2) results in a decrease in T_{VIS} of 6% (from 81.1% to 75.2%, see Figure 10 *(b)*). Nevertheless we note that it could be

possible to engineer the light transmittance at certain wavelengths in a very precise way taking advantage of the position of the well-defined and peaked thickness fringes (*e.g.* total transmittance higher than 90% in the regions of wavelength close to 390 and 480 nm for the 295 nm thick TaTO film, blue line in Figure 10 *(b)*).

4. Discussion

Optical and electrical properties of TaTO films are strongly connected to the oxygen background pressure during the PLD process, even though an annealing process is needed to crystallize the films in the anatase phase. Oxygen vacancies (V_O) are known to play a fundamental role in the electrical properties of TiO_2 because they should represent an effective doubly negative charged donor state,[50] but the reported trends in the TaTO functional properties presented above are likely related to a more complex defect chemistry. For instance, the abrupt increase in resistivity from the vacuum to the air annealing process (from 5.73×10^{-4} Ωcm up to a resistance value higher than 10 GΩ) is not easily explained only with the absence of V_O resulting from an oxygen-rich atmosphere. In fact, the incorporation of Ta as an active dopant (5% at.), due to the substitution of Ti atoms in the anatase TiO_2 cell (Ta_{Ti}), should provide a free electron concentration[54] in the order of 10^{21} cm^{-3} (in line with our data shown in Figure 5 for vacuum annealed TaTO); the amount of free electrons due to the formation of doubly positive charged oxygen vacancies (V_O) during a vacuum annealing process has been proved to be in the order of 10^{19} cm^{-3} (i.e. for vacuum annealed undoped TiO_2, see Figure 5). Therefore, in agreement with what is supported by Huy *et al.*,[15] the lack (or the reduced amount) of V_O that should be associated to oxygen-rich conditions cannot explain alone the highly insulating properties obtained for TaTO air annealed films or the drop in conductivity for higher oxygen deposition pressures (see Figure 6); nevertheless, we are aware that this has to be just considered as a too simple approach to a complex problem. For instance, the possibility that the insertion of Ta in the anatase matrix could itself

affect the concentration of produced oxygen vacancies in reducing atmosphere with respect to the undoped TiO_2 should also be taken into account. One possible explanation to the oxygen-related loss of conductivity suggested by Huy *et al.,*[15] is that the solubility of Ta in the anatase lattice is reduced in oxygen-rich conditions, leading to the formation of the non-doping Ta_2O_5 phase. However, O-rich conditions are expected to reduce only slightly the Ta solubility (and the number of Ta_{Ti} defects);[28,31,32] we observe that in our structural characterization we did not collect any experimental evidence of Ta segregated phases (see Section 3.1).

In this work we are not aiming to fully clarify this aspect, but still we can infer that there should be a non-obvious interplay of different defects (*e.g.* oxygen - titanium - tantalum) governing the electrical (and optical) properties. In a recent work Qi *et al.*[34] have discussed how Ti vacancies could play an important role in the defect chemistry of TaTO. These defects can actually act as "electron killers" and it has been shown that growing TiO_2-based films under oxygen rich condition should promote the occurrence of cationic vacancies and oxygen interstitials.[27,55] The coupling between a decreasing concentration of V_O and the occurrence of an increasing amount of electron "killer-defects" in the anatase cell as the oxygen deposition pressure is increased could be related to the decrease in the charge carrier density reported in Figure 6 (from 1.21×10^{21} cm^{-3} to 9.26×10^{19} cm^{-3} when moving from 1 Pa to 2.25 Pa). Still it is difficult to state if the defect concentration in the crystal lattice is fixed by the deposition process, and to which extent defects can be ruled by the annealing process. A study on thermodynamics of defects formation at a given annealing temperature and in different oxygen partial pressures would be recommended for this material, in order to clarify the kind of defects involved and the kinetics of the formation process.

On the other hand, also the mobility of the vacuum annealed TaTO samples has been shown to be connected to the oxygen background pressure during the deposition process (Figure 6). This trend

could be linked to the structural properties of the films: the presence of circular macro-cracks only observed on the surface of the TaTO deposited at 1 Pa (Figure 4 *(a)*), could explain its significant drop in electron mobility; the decrease seen for deposition pressures higher than 1.25 Pa, is likely related to the decrease of the crystalline domain size in both vertical and horizontal direction revealed by XRD and optical microscope analysis (Figure 3 *(a)* and Figure 4). Nevertheless the role of an increased concentration of the above mentioned "killer-defects" with the increase of oxygen deposition pressure could also contribute to both the decrease in the electron mobility and the mean crystalline size and should be considered.

In Section 3.1 we mentioned the presence of a shift of XRD reflections for vacuum annealed TaTO with respect to undoped TiO_2 films, dependent on the oxygen deposition pressure (see Figure 3 *(a)*). In Figure 11 we report the anatase cell parameters calculated from (101) and (200) XRD peak positions evaluated in grazing incident angle configuration for vacuum and air annealed films (TiO_2 and TaTO 1.25 Pa).

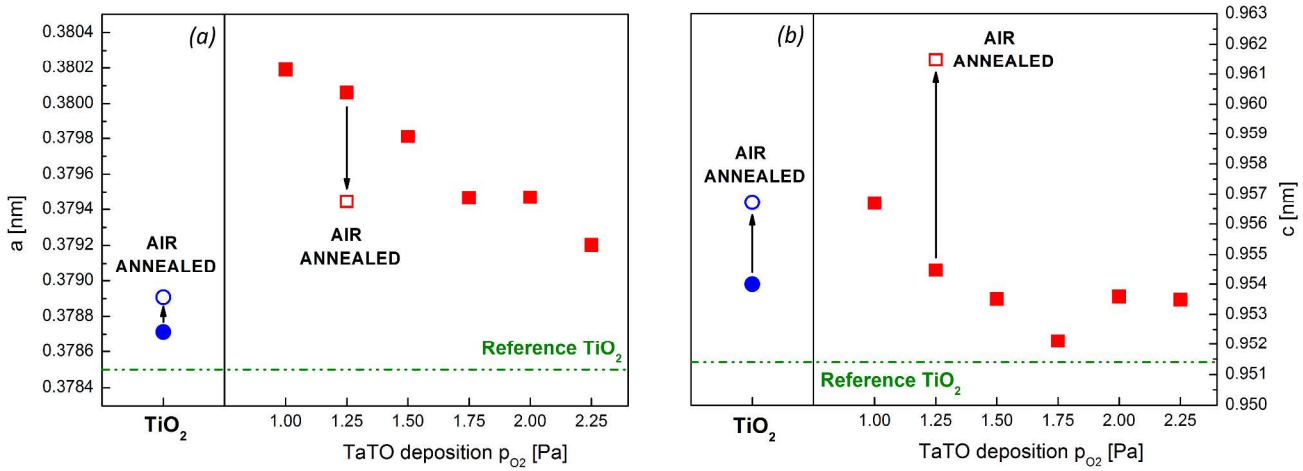

Figure 11. Anatase cell parameters (a and c respectively in *(a)* and *(b)*) evaluated for TiO_2 (blue circles) and TaTO (red squares) vacuum (filled) and air (TiO_2 and 1.25 Pa TaTO - empty) annealed films. TaTO cell parameters are plotted as a function of the oxygen

background pressure during the deposition process. The green dotted line represent the reference values for a nominally pure anatase TiO_2.[56]

A comparison between doped and undoped vacuum annealed films shows that both a and c anatase cell parameters (presented in Figure 11 *(a)* and *(b)* respectively) are generally larger for TaTO films: this could be related to a lattice expansion due to Ta incorporation in Ti substitutional sites, as commented above. Nevertheless, it is possible to notice that both a and c parameters are slightly decreasing (approaching the values for the vacuum annealed TiO_2 cell) with increasing p_{O2}; this observation could be related to a decreasing amount of oxygen vacancies as the deposition pressure is increased in TaTO thin films. It is known from theoretical calculations that V_O are thought to give a small lattice distortion in the TiO_2 anatase cell, but it is plausible that a strong interplay between V_O and substitutional Ta takes place.[57,58] The presence of a decreasing amount of V_O as the deposition pressure is increased is in line also with the transmittance data shown in Figure 8. Nevertheless when the crystallization process is performed in air, on TaTO (1.25 Pa p_{O2}) there is an increment in c coupled with a decrease in a; in this case the change in the lattice parameters is difficult to explain only as a lack of V_O in the crystal lattice and it is likely related to the presence of different defects induced by the annealing in the presence of oxygen (e.g. Ti vacancies, O interstitials). Finally, looking at the undoped TiO_2, it is possible to note that the mismatch with respect to the nominally pure anatase cell parameters (green line in Figure 11[56]), is increasing for the sample annealed in air atmosphere; this evidence could again be related to the above mentioned presence of oxygen-induced defects.

We also evaluated the optical gap for the vacuum annealed TaTO films by means of Tauc plots. Because of the indirect band gap of TiO_2, $(\alpha h\nu)^{0.5}$ versus hν was plotted in the proximity of the absorption onset. The absorption coefficient α was evaluated from transmittance and reflectance spectra via the Lambert-Beer law (with $\alpha = -1/d\ (T/(1-R))$). Thus the optical band gap ΔE_G was extrapolated with the intercept in the energy axis using a linear fit. The obtained optical energy gaps for the TaTO

vacuum annealed films deposited at different oxygen background pressures are plotted as a function of the charge carrier density (Figure 12), since we aim at evaluating the possible presence of a Moss-Burstein effect due to the filling of the conduction band by free carriers.[59]

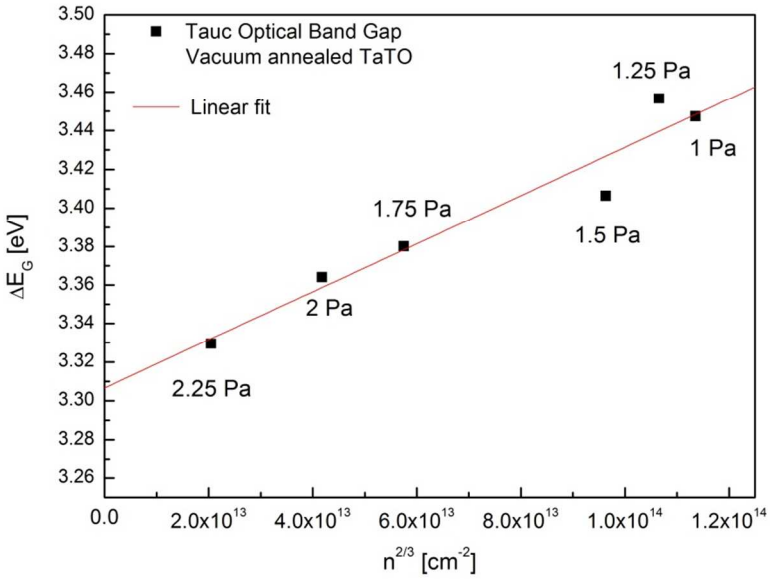

Figure 12. Tauc optical band gap as a function of $n^{2/3}$ for vacuum annealed TaTO films deposited at different oxygen partial pressures. The charge carrier densities were taken from Hall effect measurements reported in Figure 6.

As observed in Figure 12, ΔE_G shows a trend as a function of the charge carrier density. The reliability of these data is confirmed by the evaluation of the energy value obtained by the y-axis intercept of the linear fit, i.e. 3.31 eV. In fact this value is in line with the band gap of anatase TiO_2, which is known to be around 3.2 – 3.4 eV.[9,10] Since in a simplified Drude model picture the shift in the optical band gap should obey the equation:

$$\Delta E_G = \hbar^2 / 2m^* (3\pi^2 n)^{2/3}$$

from the slope of the linear fit we are able to estimate the electron effective mass to be $m^* = 2.9m_0$, where m_0 is the electron rest mass. The evaluated m^* should be considered as a combination of the two different values of effective mass reported for the anisotropic anatase cell, the orthogonal m_x^* and

parallel m_z^* (with respect to the tetragonal axis), since it is likely that the electron path is almost randomly oriented with respect to the cell. While m_x^* was evaluated to be in the range 0.4 - 0.6 m_0, which is actually the usual TCO range,[60] m_z^* is definitely higher since no value smaller than 3.5 m_0 has ever been theoretically deduced from anatase band structure calculations.[15,61] According to these values, the electron effective mass evaluated in this work from optical measurements seems to be consistent. Nonetheless this value should be read just as an estimate since it does not take into account the many-body effects and the nonparabolicity of the conduction band, which usually lead an overestimate of the deduced m^*. Moreover, based on the comparison between experimental data and DFT calculations, Huy *et al.*[15,61] found a severe increase of m_z^* with increasing charge carrier concentration for both NTO and TaTO. The enhancement of the optical effective mass with carrier density in the direction parallel to the main axis of the Ta-doped system was calculated to be less than 60% of that in Nb-doped anatase.[15] Since a higher m^* should be detrimental for charge carrier mobility, the large values of the mobility reported in this work for TaTO polycrystalline films with respect to NTO ones could be possibly explained in this way (up to $\mu = 13.0$ $cm^2V^{-1}s^{-1}$ for $n = 8.61\times10^{20}$ cm^{-3}). This represents a 40% improvement with respect to the highest mobility values reported for a polycrystalline NTO film ($\mu = 9.1$ $cm^2V^{-1}s^{-1}$ for $n = 1.7\times10^{21}$ cm^{-3}), interestingly obtained for a (001) preferential orientation.[51] Of course we are aware that in polycrystalline films scattering by grain boundaries can play a relevant role in determining electron mobility; however, no evidence of mobility values higher than 8 $cm^2V^{-1}s^{-1}$ has been reported for randomly oriented polycrystalline NTO films.

Finally we discuss the light absorption by the gas of conduction carriers: the plasma wavelength λ_p can be evaluated from the relation:

$$\lambda_p = 2\pi c \left(\frac{\varepsilon_0 \varepsilon_\infty m^*}{n_e e^2} \right)^{1/2}$$

where ε_0, ε_∞, c, m^*, and e denote the dielectric constant of vacuum, the high-frequency permittivity, the speed of light, the effective mass, and the electronic charge, respectively. Since ε_∞ was reported to be equal to 5.9 for TiO_2,[62] and the electron effective mass was estimated in this work to be $m^* = 2.9m_0$, the maximum absorption by electrons in the conduction band can be estimated to be at a wavelength of 4160 nm for $n = 1.1\times10^{21}$ cm^{-3}. This value seems to be consistent with the transmittance spectra shown in Figure 9, although it was not possible to experimentally verify the maximum λ_p absorption, due to the upper limit of our experimental setup ($\lambda_{max} = 2000$ nm). This high value of λ_p is definitely an advantage for TCO applications, since for other materials such as ZnO, In_2O_3 and SnO_2 based TCOs, the useful number of the free electrons is limited by a shift ($\propto \sqrt{m^*}$) of λ_p in the visible region.[63] This makes TaTO a very interesting material for application as a TCO in solar cells, in which an enhanced transmittance at longer wavelengths with respect to the visible region (400 – 1100 nm) is a preferred property.[14]

5. Conclusions

We have performed a thorough investigation of the electrical and optical properties of Ta-doped TiO_2 polycrystalline films in order to understand and control the real potentialities of this novel TCO. It has been shown how it is possible to combine low resistivity values of the order of 5×10^{-4} Ωcm with mean transmittance in the visible region exceeding 80%. We discussed the effect of the oxygen background pressure during the deposition process and the role of the post annealing atmosphere.

We were able to estimate the optical electron effective mass and we analyzed the obtained data in view of the high mobility values obtained for our polycrystalline thin films (up to 13 $cm^2V^{-1}s^{-1}$). This shows how Ta could have definite advantages with respect to the most investigated Nb as a TiO_2 dopant for TCO applications.

References:

1. O'Regan, B.; Gratzel, M. A Low-Cost, High-Efficiency Solar Cell Based on Dye-Sensitized Colloidal TiO_2 Films. *Nature*, **1991**, *353,* 737-740.
2. Lee, M.M.; Teuscher, J.; Miyasaka, T.; Murakami, T. N.; Snaith, H. J. Efficient Hybrid Solar Cells Based on Meso-Superstructured Organometal Halide Perovskites. *Science*, **2012**, *338,* 643-647.
3. Gondoni, P.; Mazzolini, P.; Russo, V.; Petrozza, A.; Srivastava, A. K.; Li Bassi, A.; Casari, C. S. Enhancing Light Harvesting by Hierarchical Functionally Graded Transparent Conducting Al-Doped ZnO Nano- and Mesoarchitectures. *Sol. Energ. Mat. and Sol. C.*, **2014**, *128,* 248-253.
4. Gong, J.W., Liang, J.; Sumathy, K. Review on Dye-Sensitized Solar Cells (DSSCs): Fundamental Concepts and Novel Materials. *Renew. Sust. Energ. Rev.*, **2012**, *16,* 5848-5860.
5. Rühle, S.; Dittrich T. Investigation of the Electric Field in TiO_2/FTO Junctions Used in Dye-Sensitized Solar Cells by Photocurrent Transients. *J. Phys. Chem. B*, **2005**, *109,* 9522-9526.
6. Snaith, H.J.; Grätzel M. The Role of a "Schottky Barrier" at an Electron-Collection Electrode in Solid-State Dye-Sensitized Solar Cells. *Adv. Mater.*, **2006**, *18,* 1910-1914.
7. Xue, G.; Guo, Y.; Yu, T.; Guan, J.; Yu, X.; Zhang, J.; Liu, J.; Zou, Z. Degradation Mechanisms Investigation for Long-Term Thermal Stability of Dye-Sensitized Solar Cells. *Int. J. Electrochem. Sc.*, **2012**, *7,* 1496-1511.
8. Hagfeldt, A.; Boschloo, G.; Sun, L.; Kloo, L.; Pettersson, H. Dye-Sensitized Solar Cells. *Chem. Rev.*, **2010**, *110,* 6595-6663.
9. Tang, H.; Berger, H.; Schmid, P. E.; Lévy, F.; Burri, G. Photoluminescence in TiO_2 Anatase Single Crystals. *Solid State Commun.*, **1993**, *87,* 847-850.

10. Tang, H.; Lévy, F.; Berger, H.; Schmid, P. E. Urbach Tail of Anatase TiO_2. *Phys. Rev. B*, **1995**, *52,* 7771-7774.

11. Furubayashi, Y.; Hitosugi, T.; Yamamoto, Y.; Inaba, K.; Kinoda, G.; Hirose, Y.; Shimada, T.; Hasegawa, T. A Transparent Metal: Nb-Doped Anatase TiO_2. *Appl. Phys. Lett.*, **2005**, *86,* 252101.

12. Hitosugi, T.; Furubayashi, Y.; Ueda, A.; Itabashi, K.; Inaba, K.; Hirose, Y.; Kinoda, G.; Yamamoto, Y.; Shimada, T.; Hasegawa, T. Ta-Doped Anatase TiO_2 Epitaxial Film as Transparent Conducting Oxide. *Jpn. J. Appl. Phys. 2*, **2005**, *44,* L1063-L1065.

13. Minami, T. Transparent Conducting Oxide Semiconductors for Transparent Electrodes. *Semicond. Sci. Tech.*, **2005**, *20,* S35-S44.

14. Ellmer, K. Past Achievements and Future Challenges in the Development of Optically Transparent Electrodes. *Nat. Photonics*, **2012**, *6,* 809-817.

15. Huy, H.A.; Aradi, B.; Frauenheim, T.; Deák, P. Comparison of Nb- and Ta-Doping of Anatase TiO_2 for Transparent Conductor Applications. *J. Appl. Phys.*, **2012**, *112,* 016103.

16. Furubayashi, Y.; Yamada, N.; Hirose, Y.; Yamamoto, Y.; Otani, M.; Hitosugi, T.; Shimada, T.; Hasegawa, T. Transport Properties of d-Electron-Based Transparent Conducting Oxide: Anatase $Ti_{1-x}Nb_xO_2$. *J. Appl. Phys.*, **2007**, *101,* 093705.

17. Hitosugi, T.; Ueda, A.; Nakao, S.; Yamada, N.; Furubayashi, Y.; Hirose, Y.; Shimada, T.; Hasegawa, T., Fabrication of Highly Conductive $Ti_{1-x}Nb_xO_2$ Polycrystalline Films on Glass Substrates Via Crystallization of Amorphous Phase Grown by Pulsed Laser Deposition. *Appl. Phys. Lett.*, **2007**, *90,* 212106.

18. Yamada, N.; Hitosugi, T.; Hoang, N. L. H.; Furubayashi, Y.; Hirose, Y.; Shimada, T.; Hasegawa, T. Fabrication of Low Resistivity Nb-Doped TiO_2 Transparent Conductive

Polycrystalline Films on Glass by Reactive Sputtering. *Jpn. J. Appl. Phys. 1*, **2007**, *46,* 5275-5277.

19. Dabney, M.S.; van Hest, M. F. A. M.; Teplin, C. W.; Arenkiel, S. P.; Perkins, J. D.; Ginley, D. S. Pulsed Laser Deposited Nb Doped TiO_2 as a Transparent Conducting Oxide. *Thin Solid Films*, **2008**, *516,* 4133-4138.

20. Hitosugi, T; Kamisaka, H.; Yamashita, K.; Nogawa, H.; Furubayashi, Y.; Nakao, S.; Yamada, N.; Chikamatsu, A.; Kumigashira, H.; Oshima, M.; et al. Electronic Band Structure of Transparent Conductor: Nb-Doped Anatase TiO_2. *Appl. Phys. Express*, **2008**, *1,* 1112031-1112033.

21. Hitosugi, T.; Ueda, A.; Nakao, S.; Yamada, N.; Furubayashi, Y.; Hirose, Y.; Konuma, S.; Shimada, T.; Hasegawa, T. Transparent Conducting Properties of Anatase $Ti_{0.94}Nb_{0.06}O_2$ Polycrystalline Films on Glass Substrate. *Thin Solid Films*, **2008**, *516,* 5750-5753.

22. Yamada, N.; Hitosugi, T.; Hoang, N. L. H.; Furubayashi, Y.; Hirose, Y.; Konuma, S.; Shimada, T.; Hasegawa, T. Structural, Electrical and Optical Properties of Sputter-Deposited Nb-Doped TiO_2 (TNO) Polycrystalline Films. *Thin Solid Films*, **2008**, *516,* 5754-5757.

23. Lee, S.; Noh, J. H.; Han, H. S.; Yim, D. K.; Kim, D. H.; Lee, J.-K.; Kim, J. Y.; Jung, H. S.; Hong, K. S. Nb-Doped TiO_2: A New Compact Layer Material for TiO_2 Dye-Sensitized Solar Cells. *J. Phys. Chem. C*, **2009**, *113,* 6878-6882.

24. Tonooka, K.; Chiu, T.-W.; Kikuchi, N. Preparation of Transparent Conductive TiO_2:Nb Thin Films by Pulsed Laser Deposition. *Appl. Surf. Sci.*, **2009**, *255,* 9695-9698.

25. Yamada, N.; Hitosugi, T.; Kasai, J.; Hoang, N. L. H.; Nakao, S.; Hirose, Y.; Shimada, T.; Hasegawa, T. Direct Growth of Transparent Conducting Nb-Doped Anatase TiO_2 Polycrystalline Films on Glass. *J. Appl. Phys.*, **2009**, *105,* 123702.

26. Nogawa, H.; Chikamatsu, A.; Hirose, Y.; Nakao, S.; Kumigashira, H.; Oshima, M.; Hasegawa, T. Carrier Compensation Mechanism in Heavily Nb-Doped Anatase $Ti_{1-x}Nb_xO_{2+\delta}$ Epitaxial Thin Films. *J. Phys. D Appl. Phys.*, **2011**, *44,* 365404.

27. Lee, H.-Y.; Robertson J. Doping and Compensation in Nb-Doped Anatase and Rutile TiO_2. *J. Appl. Phys.*, **2013**, *113,* 213706.

28. Neubert, M.; Cornelius, S.; Fiedler, J.; Gebel, T.; Liepack, H.; Kolitsch, A.; Vinnichenko, M. Overcoming Challenges to the Formation of High-Quality Polycrystalline TiO_2:Ta Transparent Conducting Films by Magnetron Sputtering. *J. Appl. Phys.*, **2013**, *114,* 083707.

29. Ok, K.-C; Park, Y.; Chung, K.-B.; Park, J.-S. The Effect of Ta Doping in Polycrystalline TiO_x and the Associated Thin Film Transistor Properties. *Appl. Phys. Lett.*, **2013**, *103,* 213501.

30. Wu, B.B.; Pan, F. M.; Yang, Y. E. Annealing Effect of Pulsed Laser Deposited Transparent Conductive Ta-Doped Titanium Oxide Films. *Chinese Phys. Lett.*, **2011**, *28,* 118102.

31. Osorio-Guillén, J.; Lany, S.; Zunger, A. Atomic Control of Conductivity Versus Ferromagnetism in Wide-Gap Oxides Via Selective Doping: V, Nb, Ta in Anatase TiO_2. *Phys. Rev. Lett.*, **2008**, *100,* 036601.

32. Rusydi, A.; Dhar, S.; Barman, A. R.; Ariando; Qi, D.-C.; Motapothula, M.; Yi, J. B.; Santoso, I.; Feng, Y. P.; Yang, K.; et al. Cationic-Vacancy-Induced Room-Temperature Ferromagnetism in Transparent, Conducting Anatase $Ti_{1-x}Ta_xO_2$ ($x\sim0.05$) Thin Films. *Philos. T. Roy. Soc. A*, **2012**, *370,* 4927-4943.

33. Yamamoto, T.; Ohno T. Screened Hybrid Density Functional Study on Nb- and Ta-Doped TiO_2. *Phys. Rev. B*, **2012**, *85,* 033104.

34. Qi, D.C.; Barman, A. R.; Debbichi, L.; Dhar, S.; Santoso, I.; Asmara, T. C.; Omer, H.; Yang, K.; Krüger, P.; Wee, A. T. S.; et al. Cationic Vacancies and Anomalous Spectral-Weight

Transfer in $Ti_{1-x}Ta_xO_2$ Thin Films Studied Via Polarization-Dependent Near-Edge X-Ray Absorption Fine Structure Spectroscopy. *Phys. Rev. B*, **2013**, *87,* 245201.

35. Hitosugi, T.; Yamada, N.; Nakao, S.; Hirose, Y.; Hasegawa, T. Properties of TiO_2-Based Transparent Conducting Oxides. *Phys. Status Solidi A*, **2010**, *207,* 1529-1537.

36. Hitosugi, T.; Ueda, A.; Furubayashi, Y.; Hirose, Y.; Konuma, S.; Shimada, T.; Hasegawa, T. Fabrication of TiO_2-Based Transparent Conducting Oxide Films on Glass by Pulsed Laser Deposition. *Jpn. J. Appl. Phys. 2*, **2007**, *46,* L86-L88.

37. Hoang, N.L.H.; Yamada, N.; Hitosugi, T.; Kasai, J.; Nakao, S.; Shimada, T.; Hasegawa, T. Low-Temperature Fabrication of Transparent Conducting Anatase Nb-Doped TiO_2 Films by Sputtering. *Appl. Phys. Express*, **2008**, *1,* 1150011-1150013.

38. Hitosugi, T.; Yamada, N.; Hoang, N. L. H.; Kasai, J.; Nakao, S.; Shimada, T.; Hasegawa, T. Fabrication of TiO_2-Based Transparent Conducting Oxide on Glass and Polyimide Substrates. *Thin Solid Films*, **2009**, *517,* 3106-3109.

39. Sato, Y.; Sanno, Y.; Tasaki, C.; Oka, N.; Kamiyama, T.; Shigesato, Y. Electrical and Optical Properties of Nb-Doped TiO_2 Films Deposited by DC Magnetron Sputtering Using Slightly Reduced Nb-Doped TiO_{2-x} Ceramic Targets. *J. Vac. Sci. Technol. A*, **2010**, *28,* 851-855.

40. Liu, J.; Zhao, X.; Duan, L.; Cao, M.; Sun, H.; Shao, J.; Chen, S.; Xie, H.; Chang, X.; Chen, C. Influence of Annealing Process on Conductive Properties of Nb-Doped TiO_2 Polycrystalline Films Prepared by Sol–Gel Method. *Appl. Surf. Sci.*, **2011**, *257,*10156-10160.

41. Kim, H. Transparent Conducting Oxide Films. In *Pulsed laser deposition of thin films: applications-led growth of functional materials*; Eason, R.; John Wiley & Sons, Inc.: Hoboken, NJ, 2007; pp. 236-260.

42. Balachandran, U.; Eror N. G. Raman Spectra of Titanium Dioxide. *J. Solid State Chem.*, **1982**, *42,* 276-282.

43. Li Bassi, A.; Cattaneo, D.; Russo, V.; Bottani, C. E.; Barborini, E.; Mazza, T.; Piseri, P.; Milani, P.; Ernst, F. O.; Wegner, K.; et al. Raman Spectroscopy Characterization of Titania Nanoparticles Produced by Flame Pyrolysis: The Influence of Size and Stoichiometry. *J. Appl. Phys.*, **2005**, *98,* 074305.

44. Oliver, P. M.; Watson, G. W.; Toby Kelsey, E.; Parker, S. C. Atomistic Simulation of the Surface Structure of the TiO_2 Polymorphs Rutile and Anatase. *J. Mater. Chem.*, **1997**, *7,* 563-568.

45. Yang, C.; Hirose, Y.; Nakao, S.; Hasegawa, T. C-Axis-Oriented Growth of Anatase TiO_2 Thin Films on Glass Substrate with $SrTiO_3$/TiN Template. *J. Crys. Growth*, **2013**, *376,* 66-69.

46. Dy, E.; Hui, R.; Zhang, J.; Liu, Z.-S.; Shi, Z. Electronic Conductivity and Stability of Doped Titania ($Ti_{1-x}M_xO_2$, M = Nb, Ru, and Ta)—A Density Functional Theory-Based Comparison. *J. Phys. Chem. C*, **2010**, *114,* 13162-13167.

47. Pore, V.; Ritala, M.; Leskelä, M.; Saukkonen, T.; Järn, M. Explosive Crystallization in Atomic Layer Deposited Mixed Titanium Oxides. *Cryst. Growth Des.*, **2009**, *9,* 2974-2978.

48. Tachikawa, T.; Minohara, M.; Nakanishi, Y.; Hikita, Y.; Yoshita, M.; Akiyama, H.; Bell, C.; Hwang, H.Y. Metal-to-Insulator Transition in Anatase TiO_2 Thin Films Induced by Growth Rate Modulation. *Appl. Phys. Lett.*, **2012**, *101,* 022104.

49. Chen, D.-m.; Xu, G.; Miao, L.; Nakao, S.; Jin, P. Sputter Deposition and Computational Study of M-TiO_2 (M = Nb, Ta) Transparent Conducting Oxide Films. *Surf. Coat. Tech.*, **2011**, *206,* 1020-1023.

50. Deák, P.; Aradi, B.; Frauenheim, T. Quantitative Theory of the Oxygen Vacancy and Carrier Self-Trapping in Bulk TiO_2. *Phys. Rev. B*, **2012**, *86,* 195206.

51. Yamada, N.; Shibata, T.; Taira, K.; Hirose, Y.; Nakao, S.; Ngoc, L. H. H.; Hitosugi, T.; Shimada, T.; Sasaki, T.; Hasegawa, T. Enhanced Carrier Transport in Uniaxially (001)-Oriented

Anatase $Ti_{0.94}Nb_{0.06}O_2$ Films Grown on Nanosheet Seed Layers. *Appl. Phys. Express*, **2011**, *4,* 045801.

52. Brudnik, A.; Czternastek, H.; Zakrzewska, K.; Jachimowski, M. Plasma-Emission-Controlled DC Magnetron Sputtering of TiO_{2-x} Thin Films. *Thin Solid Films*, **1991**, *199,* 45-58.

53. Poelman, H.; Tomaszewski, H.; Poelman, D.; Depla, D.; De Gryse, R. Effect of the Oxygen Deficiency of Ceramic TiO_{2-x} Targets on the Deposition of TiO_2 Thin Films by DC Magnetron Sputtering. *Surf. Interface Anal.*, **2004**, *36,* 1167-1170.

54. Deák, P.; Aradi, B.; Frauenheim, T. Polaronic Effects in TiO_2 Calculated by the HSE06 Hybrid Functional: Dopant Passivation by Carrier Self-Trapping. *Phys. Rev. B*, **2011**, *83,* 155207.

55. Zhang, S.; Ogale, S. B.; Yu, W.; Gao, X.; Liu, T.; Ghosh, S.; Das, G. P.; Wee, A. T. S.; Greene, R. L.; Venkatesan, T. Electronic Manifestation of Cation-Vacancy-Induced Magnetic Moments in a Transparent Oxide Semiconductor: Anatase Nb:TiO_2. *Adv. Mater.*, **2009**, *21,* 2282-2287.

56. Hanaor, D.A.H.; Sorrell, C. C. Review of the Anatase to Rutile Phase Transformation. *J. Mater. Sci.*, **2011**, *46,* 855-874.

57. Peng, H.; Li, J.; Li, S.-S.; Xia, J.-B. Possible Origin of Ferromagnetism in Undoped Anatase TiO_2. *Phys. Rev. B*, **2009**, *79,* 092411.

58. Kim, D.; Hong, J.; Park, Y. R.; Kim, K. J. The Origin of Oxygen Vacancy Induced Ferromagnetism in Undoped TiO_2. *J. Phys. Condens. Matter*, **2009**, *21,* 195405.

59. Burstein, E. Anomalous Optical Absorption Limit in InSb. *Phys. Rev.*, **1954**, *93,* 632-633.

60. Gondoni, P.; Ghidelli, M.; Di Fonzo, F.; Carminati, M.; Russo, V.; Bassi, A. L.; Casari, C. S. Structure-Dependent Optical and Electrical Transport Properties of Nanostructured Al-Doped ZnO. *Nanotechnology*, **2012**, *23,* 365706.

61. Huy, H.A.; Aradi, B.; Frauenheim, T.; Deák, P. Calculation of Carrier-Concentration-Dependent Effective Mass in Nb-Doped Anatase Crystals of TiO_2. *Phys. Rev. B*, **2011**, *83,* 155201.

62. Gonzalez, R. J.; Zallen, R.; Berger, H. Infrared Reflectivity and Lattice Fundamentals in Anatase TiO_2. *Phys. Rev. B*, **1997**, *55,* 7014-7017.

63. Gondoni, P.; Ghidelli, M.; Di Fonzo, F.; Russo, V.; Bruno, P.; Marti-Rujas, J.; Bottani, C. E.; Bassi, A. L.; Casari, C. S. Structural and Functional Properties of Al:ZnO Thin Films Grown by Pulsed Laser Deposition at Room Temperature. *Thin Solid Films*, **2012**, *520,* 4707-4711.

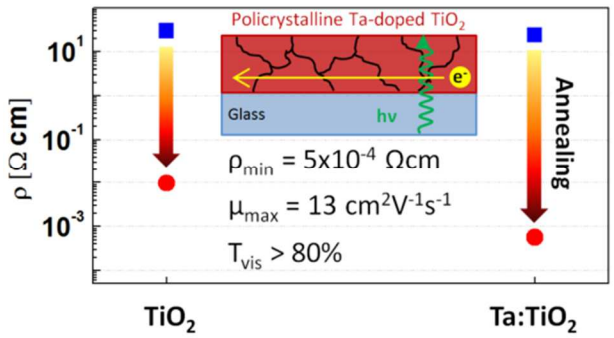

For Table of Contents Only

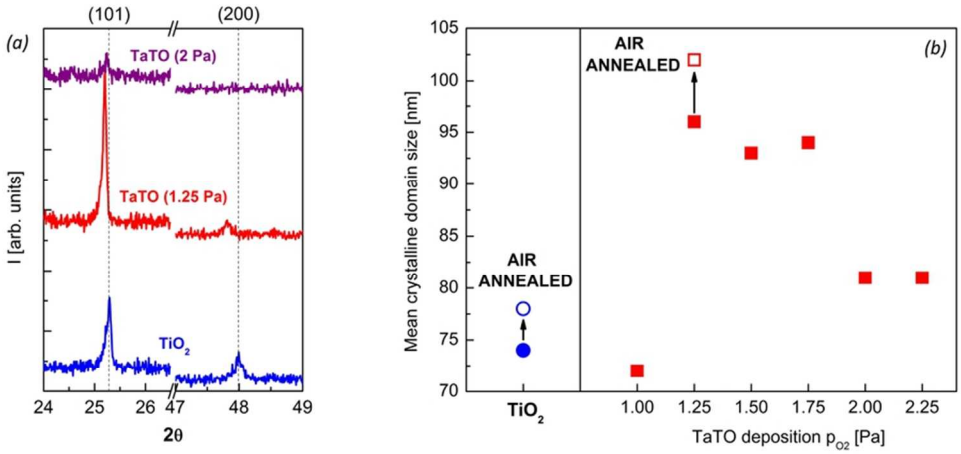

Fig 3
79x36mm (300 x 300 DPI)

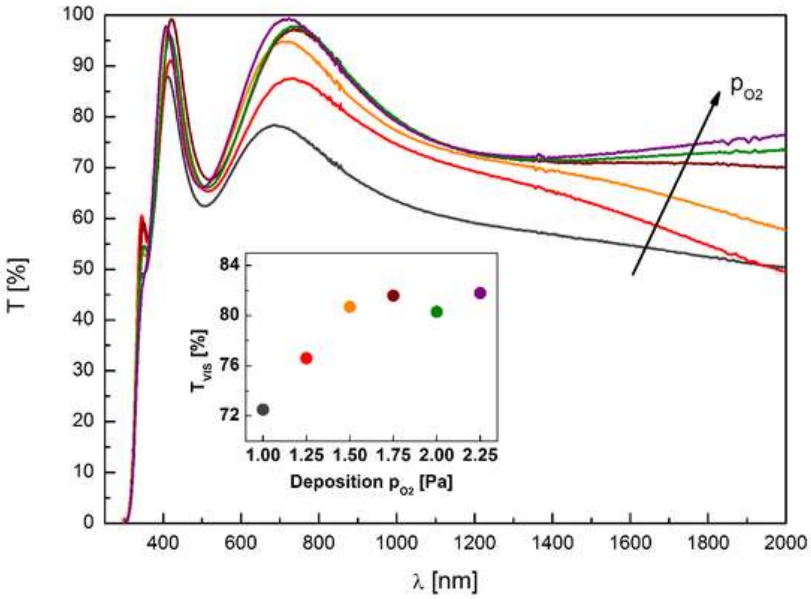

Fig 8
56x39mm (300 x 300 DPI)

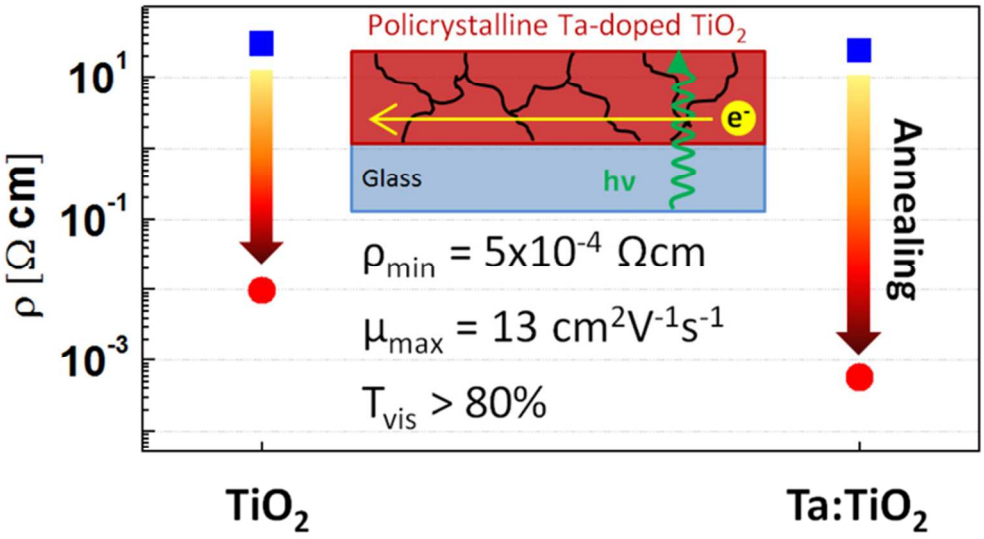

TOC graphics
33x18mm (600 x 600 DPI)